Predictive Trailing-Edge Modulation Average Current Control in DC-DC Converters

Daniel DRĂGHICI, Dan LASCU
Politehnica University Timişoara, 300207, Romania
daniel.draghici@etc.upt.ro

***Abstract*—The paper investigates predictive digital average current control (PDACC) in dc/dc converters using trailing-edge modulation (TEM). The study is focused on the recurrence duty cycle equation and then stability analysis is performed. It is demonstrated that average current control using trailing-edge modulation is stable on the whole range of the duty cycle and thus design problems are highly reduced. The analysis is carried out in a general manner, independent of converter topology and therefore the results can then be easily applied for a certain converter (buck, boost, buck-boost, etc.). The theoretical considerations are confirmed for a boost converter first using the MATLAB program based on state-space equations and finally with the CASPOC circuit simulation package.**

***Index Terms*—Current programmed control, predictive current control, trailing-edge modulation, average current control.**

I. Introduction

Current mode control has become classical as it is intensively used with dc-dc converters [1-10]. It was also the starting point for other control techniques such as charge control [11]. Current mode control found an important application in power-factor-correction (PFC) circuits [12-14]. Analog current programmed control can be classified as peak, valley or average current control, depending on whether the maximum, the minimum or the average value of the sensed current in a period is compared to a reference and tightly controlled. It is also known that peak current control offers fast over-current switch protection [15]. In PFC applications, the peak or valley control inherently lead to line current harmonic distortion and several solutions for reducing this distortion have been proposed [10], [11] by biasing the reference waveform. On the other side, average current mode control offers the advantage of both constant frequency operation and low harmonic distortion [4].

Digital controllers have rapidly penetrated in the field of power electronics. Digital control offers some crucial advantages such as programmability, insensitivity to parameter variations and flexibility in improving performance. Naturally, digital control has been extended to current control. Predictive digital current control was first proposed by Chen, Prodic, Maksimovic and Erickson [16-17] and consequently it was rapidly extended and adopted. Different modeling approaches both in analog and in the digital domain [18-23] have been proposed. The analysis in [16] was carried out with emphasis on a boost TEM valley control and some considerations regarding other techniques were just mentioned. The paper is organized as follows: section II presents predictive digital average current control principle, in section III stability analysis is performed, MATLAB investigation of the PDACC with TEM using a state space approach is carried out in section IV, section V is devoted to verification of the theoretical aspects by circuit simulation, while conclusions are drawn in section VI.

II. Predictive Digital Average Current Control Using Trailing Edge Modulation

A. Principle

Fig. 1 shows the trailing-edge pulse-width modulation (PWM) control. The rectangular switching function $q(t)$ is obtained by comparing the control voltage $v_c(t)$ with a saw-tooth signal, $v_{saw}(t)$. In TEM the transistor is switched on at the beginning of each period of length T_s and switched off after dT_s time units. The duty cycle d can be modified increasing or decreasing the control voltage, $v_c(t)$. The transistor stays off for the rest of the period, that is $(1\text{-}d)T_s$ time units. It is clear that the rising edge of the switching function is equally spaced in time, while the falling edge could occur earlier or later during one switching cycle, depending on the value of the control voltage.

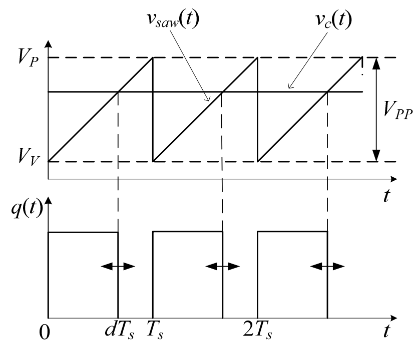

Figure 1. Trailing-edge modulation.

In PDACC technique some variables need to be sampled in the current period in order to be used in the computation of the duty cycle corresponding to the next switching cycle. The goal is to reduce to the error between the current reference I_{ref} and the average inductor current. In Fig. 2 the inductor current waveform in steady state is shown and in Fig. 3 the inductor current waveform under average current control during a transient is depicted [16]. Unless specified, capitals will denote variables in steady state (e.g. D), while noncapitalized variables will refer to dynamics (e.g. $i[n]$, d_n). Small signal perturbations will be referred using the Δ symbol in front (e.g. $\Delta i[n]$, Δd_n). The inductor current

This work was partially supported by the strategic grant POSDRU 107/1.5/S/77265 (2010) of the Ministry of Labour, Family and Social Protection, Romania, co-financed by the European Social Fund – Investing in people.

Digital Object Identifier 10.4316/AECE.2013.04019

positive slope is denoted by m_1 and for its steady-state value the symbol M_1 will be used. Similarly, $-m_2$ and $-M_2$ notations will refer to the negative inductor current slope. It is clear that both M_1 and M_2 are positive magnitudes.

B. Equations

As the inductor current is sampled at the beginning of the each switching period, notation $i[n]$ will denote the sample value of the current inductor at the beginning of the n^{th} switching cycle. The goal is to derive a relationship for the duty cycle in the $(n+1)^{th}$ cycle in terms of duty cycle d_n, such that the average point current in the $(n+1)^{th}$ cycle to be equal to the reference current. This, of course, justifies the predictive nature of the control. In order to derive the control law regarding the duty cycle, the average point at the end of the $(n+1)^{th}$ period, denoted as $i_{ave\ n+1}$ in Fig. 3, will be evaluated in terms of $i[n]$. Finally it will be imposed that this average point to be equal to the reference value, I_{ref}.

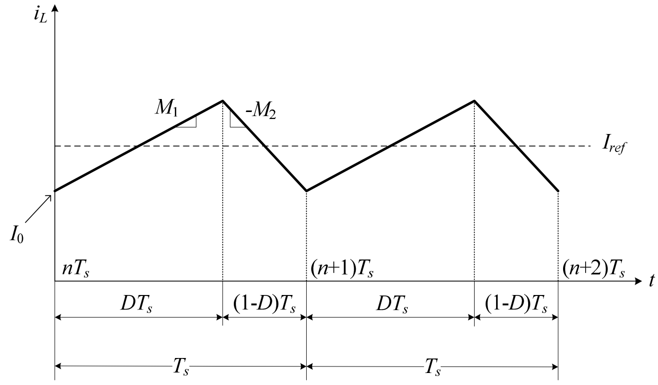

Figure 2. Inductor current waveform in steady state.

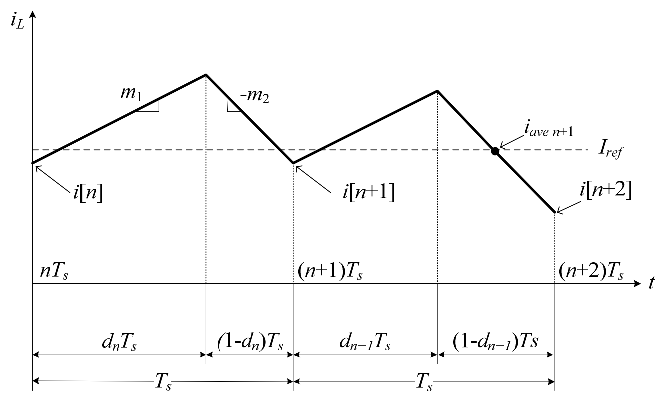

Figure 3. Inductor current waveform under PDACC during a transient.

In order to achieve this, first the sampled inductor current $i[n+1]$ is computed as a function of the previous sampled value $i[n]$ and the applied duty cycle d_n, provided that the slopes M_1 and M_2 of the inductor current waveform are known. It also known that the steady-state duty cycle D is given by:

$$D = \frac{M_2}{M_1 + M_2} \tag{1}$$

while and the slopes ratio is provided by:

$$\frac{M_2}{M_1} = \frac{D}{1-D} \tag{2}$$

Both relationships can be easily proven expressing the inductor current ripple in each topological state and equaling the results. In the most general case, the slopes m_1 and m_2 depend on the input and output voltages. Therefore the input and the output voltages need also to be sampled. For example, in a boost converter these values are:

$$m_1 = \frac{v_{in}}{L} \tag{3}$$

$$m_2 = \frac{v_o - v_{in}}{L} \tag{4}$$

From Fig. 3, because of the piecewise linear shape of the inductor current, it can be written that:

$$i[n+1] = i[n] + m_1 d_n T_s - m_2(1-d_n)T_s \tag{5}$$

Relationship (5) can be extended for the next switching cycle making $n \rightarrow n+1$:

$$i[n+2] = i[n+1] + m_1 d_{n+1} T_s - m_2(1-d_{n+1})T_s \tag{6}$$

The average point of the inductor current at the end of the $(n+1)^{th}$ cycle is equal to:

$$i_{ave\ n+1} = \frac{1}{2}[i_L((n+1)T_s + d_{n+1}T_s) + i_L((n+2)T_s)] \tag{7}$$

Using (5) and (6), the average point of the inductor current can be expressed in the form:

$$\begin{aligned} i_{ave\ n+1} = {} & i[n] + m_1 d_n T_s - m_2(1-d_n)T_s + m_1 d_{n+1} T_s - \\ & - \frac{1}{2} m_2 (1-d_{n+1})T \end{aligned} \tag{8}$$

Imposing $i_{ave\ n+1} = I_{ref}$, it results that:

$$\begin{aligned} & i[n] + m_1 d_n T_s - m_2(1-d_n)T_s + m_1 d_{n+1} T_s - \\ & - \frac{1}{2} m_2 (1-d_{n+1})T = I_{ref} \end{aligned} \tag{9}$$

From equation (9), the value of the predicted duty cycle d_{n+1} is found in the form:

$$\begin{aligned} d_{n+1} = {} & -2\frac{m_1 + m_2}{2m_1 + m_2} d_n - \frac{2}{(2m_1 + m_2)T_s}\left(i[n] - I_{ref}\right) + \\ & + 3\frac{m_2}{2m_1 + m_2} \end{aligned} \tag{10}$$

This is the general recurrence formula for the predicted duty cycle. It can be applied to any converter customizing the slopes m_1 and m_2 according to converter topology. For example, using (3) and (4), after some simple algebra the predicted duty cycle for the boost converter is given by:

$$\begin{aligned} d_{n+1} = {} & -2\frac{v_o}{v_o + v_{in}} d_n - 2\frac{L}{(v_o + v_{in})T_s}\left(i[n] - I_{ref}\right) + \\ & + 3\frac{v_o - v_{in}}{v_o + v_{in}} \end{aligned} \tag{11}$$

One easy way to check the validity of (10) is to derive the steady-state duty cycle in terms of slopes M_1 and M_2. Obviously, in steady-state the following relationships hold:

$$i[n] = I_0 \tag{12}$$

$$d_{n+1} = d_n = D \tag{13}$$

$$I_{ref} = I_0 + \frac{1}{2} M_1 DT \tag{14}$$

where I_0 is the steady-state valley current and D is the steady-state duty cycle. Substituting the values of $i[n]$, d_{n+1}, d_n and I_{ref} into (10) from relationships (12), (13) and (14) respectively and performing the calculations it results $D=M_2/(M_1+M_2)$. This is exactly the well-known relationship (1), thus confirming the correctness of (10).

III. Stability Analysis

Stability analysis can be performed based on geometrical considerations, similar to [15], chapter 12. In Fig. 4 both the steady state and the perturbed inductor current waveforms are depicted, assuming a small perturbation. The solid line represents the inductor current waveform in steady-state and the dashed line corresponds to the perturbed inductor current. Till $t=nT_s$ the converter was operating in steady-state and at $t=nT_s$ the perturbation occurs. Therefore, from the predictive control principle it easily follows that the duty cycle in the n^{th} period will still be equal to the steady-state duty cycle D,

$$d_n = D \tag{15}$$

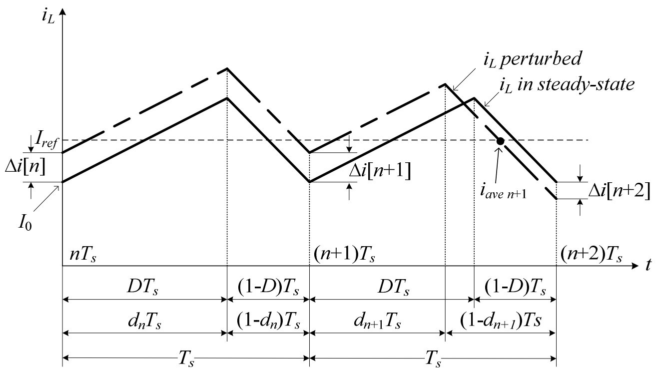

Figure 4. Inductor current under PDACC with TEM revealing the perturbations.

The first remark is that only starting with the $(n+1)^{th}$ cycle the duty cycle is perturbed. For clarity, the size of the perturbation is exaggerated. Notations $\Delta i[n]$, $\Delta i[n+1]$ and $\Delta i[n+2]$ denote the perturbations at the beginning of switching cycles n, $n+1$ and $n+2$ respectively. Because a small perturbation is assumed, the converter will operate close to steady-state, such that the slopes m_1 and m_2 may be considered unchanged and equal to their steady state values, M_1 and M_2 respectively. The purpose of this analysis is to find a relationship between the perturbation at the beginning of the $(n+2)^{th}$ switching cycle, $\Delta i[n+2]$ and the perturbation at the beginning n^{th} switching cycle, $\Delta i[n]$. Based on this recurrence, stability can be easily established examining whether $\Delta i[n+2]$ tends to 0 for large n. Obviously, from Fig.4 the perturbation $\Delta i[n]$ is defined as:

$$\Delta i[n] = i[n] - I_o \tag{16}$$

As the slopes of the two waveforms in the first topological state of the n^{th} period are equal and the duty cycle in the n^{th} period is equal to the steady-state duty cycle, as demonstrated above, it follows that the value of the perturbation at the beginning of the $(n+1)^{th}$ cycle will be equal to the perturbation at the beginning of the n^{th} cycle,

$$\Delta i[n+1] = \Delta i[n] \tag{17}$$

According to (9), as d_{n+1} is the first duty cycle after period n that takes into account the fact that the waveform is perturbed, it results that the perturbation at the beginning of the $(n+2)^{th}$ switching cycle will differ to that of the perturbation at the beginning of the n^{th} cycle. Hence:

$$i[n] = I_0 + \Delta i[n] \tag{18}$$

Taking (16) into account it results that:

$$i[n+1] = I_0 + \Delta i[n] \tag{19}$$

Based on (18), the recurrence (10) becomes:

$$d_{n+1} = -2\frac{M_1 + M_2}{2M_1 + M_2} d_n - \frac{2}{(2M_1 + M_2)T_s}\left(I_0 + \Delta i[n] - I_{ref}\right) + 3\frac{M_2}{2M_1 + M_2} \tag{20}$$

With the notation Δd_n for the duty cycle perturbation in the n^{th} period, according to this definition it is clear that:

$$d_{n+1} = \Delta d_{n+1} + D \tag{21}$$

Substituting d_n from (15), d_{n+1} from (21), I_{ref} from (14), D from (1) and $i[n]$ from (18), all into (20), after performing the calculations it results:

$$\Delta d_{n+1} = -\frac{2}{(2M_1 + M_2)T_s}\Delta i[n] \tag{22}$$

The instantaneous inductor current at beginning of the $(n+2)^{th}$ cycle is:

$$i[n+2] = I_0 + \Delta i[n+2] \tag{23}$$

On the other side, using geometrical considerations together with (5) and (6) the value of $i[n+2]$ is obtained as:

$$i[n+2] = I_0 + \Delta i[n] + M_1 d_{n+1} T_s - M_2(1 - d_{n+1})T_s \tag{24}$$

From the equality of the right hand sides in (23) and (24) it follows that:

$$\Delta i[n+2] = \Delta i[n] + M_1 d_{n+1} T_s - M_2(1 - d_{n+1})T_s \tag{25}$$

Now substituting d_{n+1} from (21) in (25), it is obtained:

$$\Delta i[n+2] = \Delta i[n] + (M_1 + M_2)T_s \Delta d_{n+1} + M_1 D T_s - M_2(1-D)T_s \tag{26}$$

Substituting Δd_{n+1} from (22) and D from (1), both in (26), the value of $\Delta i[n+2]$ can be written as:

$$\Delta i[n+2] = -\frac{\frac{M_2}{M_1}}{2 + \frac{M_2}{M_1}}\Delta i[n] \tag{27}$$

Using the value of the ratio M_2/M_1 given by (2), the right hand side of relationship (27) can be rewritten in terms of steady-state duty cycle as:

$$\Delta i[n+2] = -\frac{D}{2-D}\Delta i[n] \tag{28}$$

This is the desired recurrence and based on it stability considerations can now be easily derived. Making $n \to n+2$ in (28), it follows that:

$$\Delta i[n+4] = -\frac{D}{2-D}\Delta i[n+2] \tag{29}$$

Replacing $\Delta i[n+2]$ from (28) in (29) the value $\Delta i[n+4]$ is found:

$$\Delta i[n+4] = \left(-\frac{D}{2-D}\right)^2 \Delta i[n] \tag{30}$$

After $2k$ switching periods, the perturbation becomes:

$$\Delta i[n+2k] = \left(-\frac{D}{2-D}\right)^k \Delta i[n] \tag{31}$$

As k goes to infinity, the perturbation $\Delta i[n+2k]$ tends to 0 provided that the characteristic value $-D/(2\text{-}D)$ has the absolute value less than 1. Hence the stability condition is:

$$\left|-\frac{D}{2-D}\right| < 1 \tag{32}$$

As $0 < D < 1$ it is easy to show that

$$\left|-\frac{D}{2-D}\right| = \frac{D}{2-D} \tag{33}$$

Therefore the stability condition is equivalent to:

$$\frac{D}{2-D} < 1 \tag{34}$$

Solving (34) this immediately leads to $D<1$, that is always true. The conclusion is that predictive average current control under trailing edge modulation is unconditionally stable (no oscillation) for the whole range of the duty cycle.

IV. Verification Using State-Space Analysis

In order to evaluate the validity of the predictive average current control under trailing edge modulation, first a state-space analysis approach is carried out. The boost converter depicted in Fig. 5 is subjected to study.

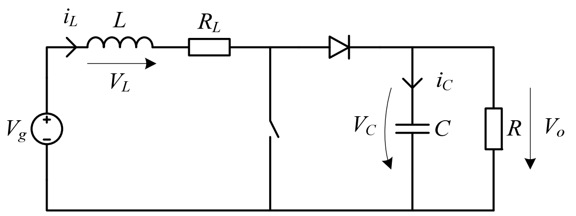

Figure 5. The boost converter investigated with PDACC.

Converter parameters are:

$$V_g = 10V;\ L = 500\mu H;\ C = 100\mu F;\ R_L = 1m\Omega;\ f_s = 40kHz \quad (35)$$

The state vector is chosen as $x=[i_L \ \ v_C]^T$. When CCM operated, the converter can be modeled by the following equations [24]:

$$\begin{cases} \dfrac{dx}{dt} = A_1 x + B_1 V_g & \text{when the switch is ON} \\ \dfrac{dx}{dt} = A_2 x + B_2 V_g & \text{when the switch is OFF} \end{cases} \quad (36)$$

where:

$$A_1 = \begin{bmatrix} -\dfrac{R_L}{L} & 0 \\ 0 & -\dfrac{1}{RC} \end{bmatrix} \quad (37)$$

$$A_2 = \begin{bmatrix} -\dfrac{R_L}{L} & -\dfrac{1}{L} \\ \dfrac{1}{C} & -\dfrac{1}{RC} \end{bmatrix} \quad (38)$$

$$B_1 = B_2 = \begin{bmatrix} \dfrac{1}{L} \\ 0 \end{bmatrix} \quad (39)$$

It is known [24] that a discrete model of the converter is described by the equation:

$$x[n+1] = \varphi_2 \varphi_1 x[n] + (\varphi_2 \psi_1 + \psi_2) V_g \quad (40)$$

where

$$\varphi_1 = e^{A_1 d_n T_S} \quad (41)$$

$$\psi_1 = A_1^{-1}(\varphi_1 - I) B_1 \quad (42)$$

$$\varphi_2 = e^{A_2 (1-d_n) T_S} \quad (43)$$

$$\psi_1 = A_2^{-1}(\varphi_2 - I) B_2 \quad (44)$$

The converter will be simulated by the use of the difference equation (40), with the duty cycle calculated according to the predictive control given by (11). An initial arbitrary duty cycle will be chosen and the simulation will be carried out long enough to overpass the initial transient. If stable operation is achieved the results in steady-state will be a sequence of constant discrete values. As unstable operation usually occurs either at $D<0.5$ or $D>0.5$, two reference current value are chosen: one value is chosen to impose operation at $D<0{,}5$ and the other to lead to $D>0.5$ operation.

The simulation results for $I_{ref}=2.5A$, ($D<0.5$) are shown in Fig. 6 while in Fig. 7, for the same current reference value, the last ten switching cycles for the inductor current are depicted. It can be seen that stable operation is achieved, as the duty cycle becomes constant after the initial transient and inductor current exhibits a typical periodic shape with a period equal to the switching period. The results for a current reference $I_{ref}=11A$, ($D>0.5$) are shown in Fig. 8 and Fig. 9 for the duty cycle and inductor current respectively. Again stable operation is achieved, thus confirming that average current control is stable at any duty cycle. The Matlab program is provided in the Appendix.

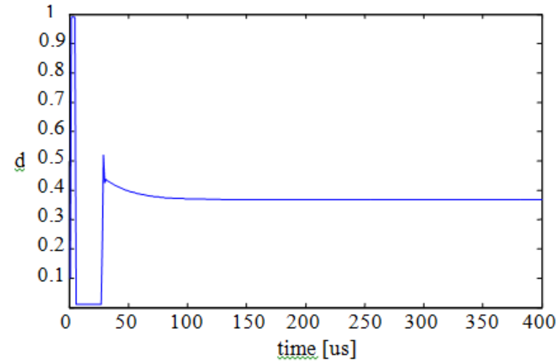

Figure 6. Duty cycle versus time for $I_{ref}=2.5A$ ($D<0.5$).

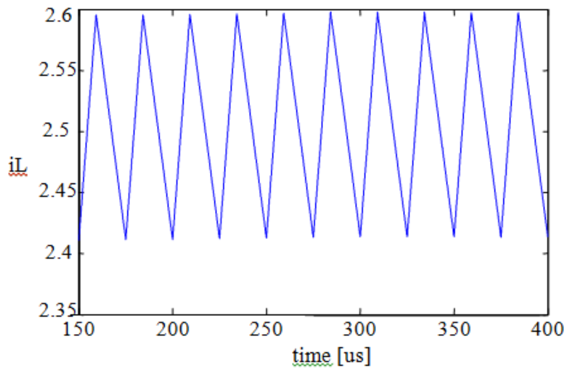

Figure 7. Inductor current for $I_{ref}=2.5A$ ($D<0.5$).

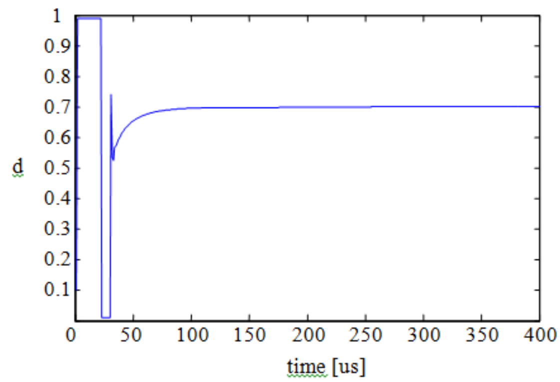

Figure 8. Duty cycle versus time for $I_{ref}=11A$ ($D>0.5$).

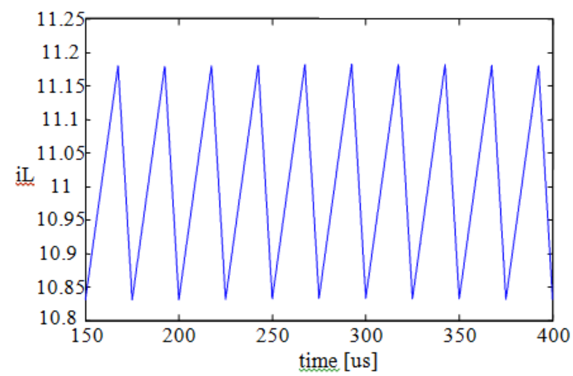

Figure 9. Inductor current for $I_{ref}=11A$ ($D>0.5$).

V. Verification Through Circuit Simulation

The CASPOC package [25] was used for simulating the boost converter with PDACC under TEM. The overall simulation schematic of a boost converter employing predictive average current control under trailing-edge modulation is presented in Fig. 10.

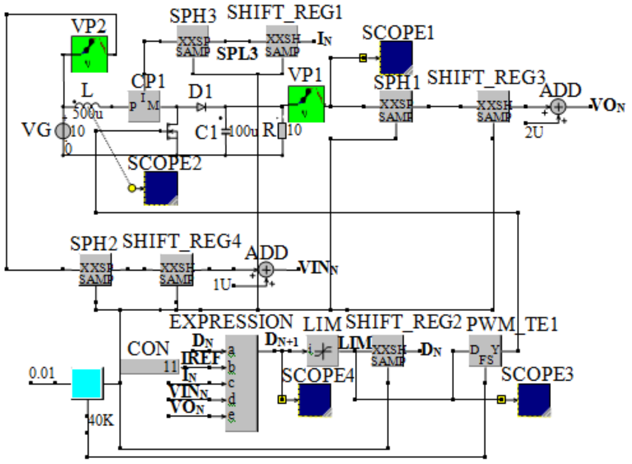

Figure 10. CASPOC schematic for the simulation of the boost converter employing PDACC under TEM.

The average inductor current must follow the reference I_{ref}. The required duty cycle for the next switching period is predicted based on the sampled current and on the sampled input and output voltages, according to (11). To implement equation (11), the EXPRESSION block in CASPOC was used. Complete details and information about the blocks used can be found in [26]. The simulated results are presented in Fig. 11, 12 and 13 for the duty cycle, inductor current and output voltage respectively. The simulation was performed employing a reference current value of 2.5*A* that forces operation at a duty cycle less than 0.5. It can be easily seen that stable operation is achieved.

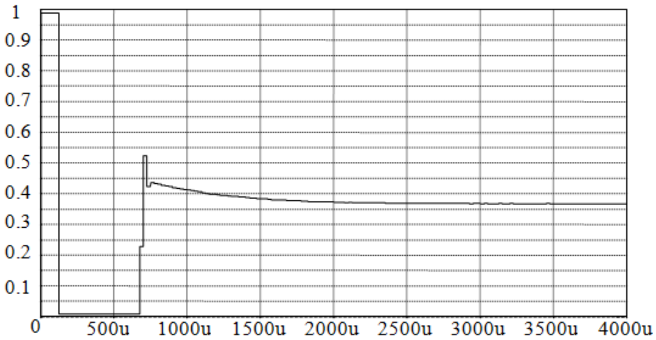

Figure 11. Duty cycle versus time for I_{ref}=2.5*A* (*D*<0.5).

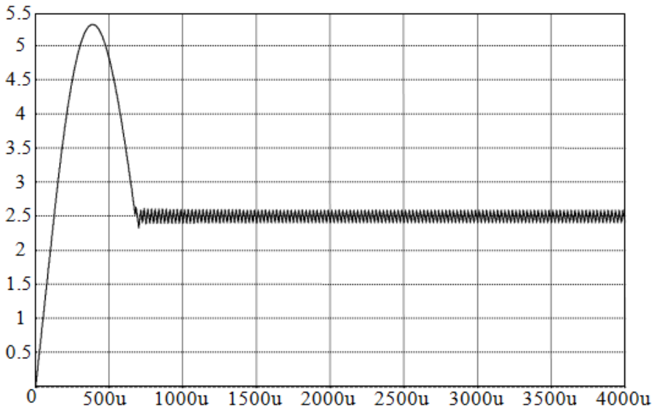

Figure 12. Inductor current for I_{ref}=2.5*A* (*D*<0.5).

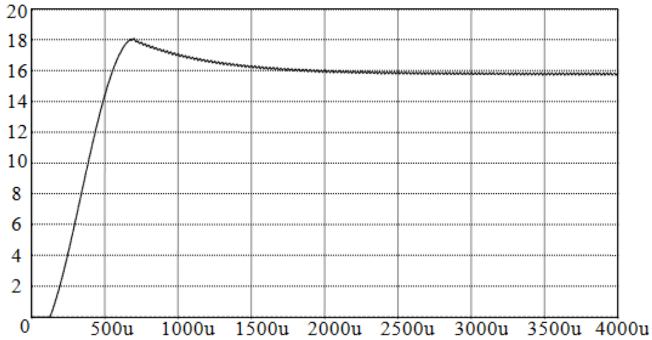

Figure 13. Output voltage for I_{ref}=2.5A (D<0.5).

With a current reference of 11*A*, that forces the operation at a duty cycle higher than 0.5, the results are shown in Fig. 14, 15 and 16. Again stable operation of the converter is achieved. Moreover, in both situations it can be seen that the control is correctly performed as the average value of the inductor current tightly follows the reference current

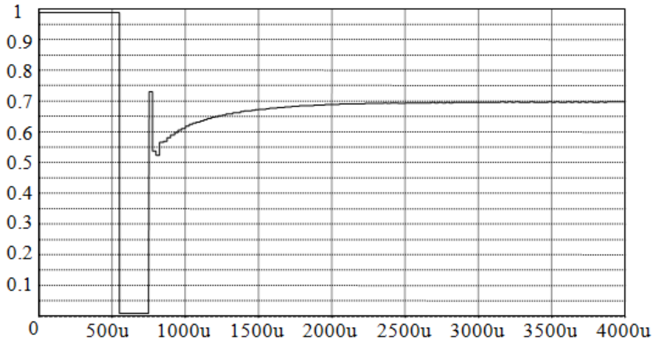

Figure 14. Duty cycle versus time for I_{ref}=11*A* (*D*>0.5).

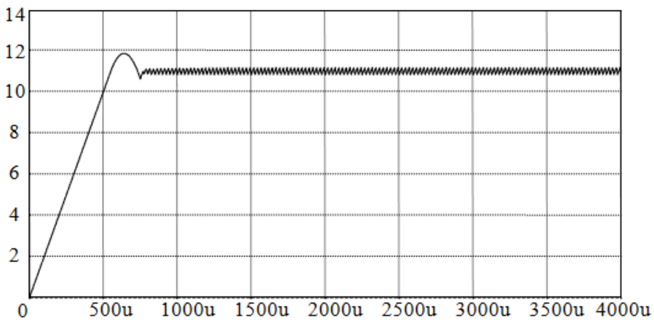

Figure 15. Inductor current for I_{ref}=11*A* (*D*>0.5).

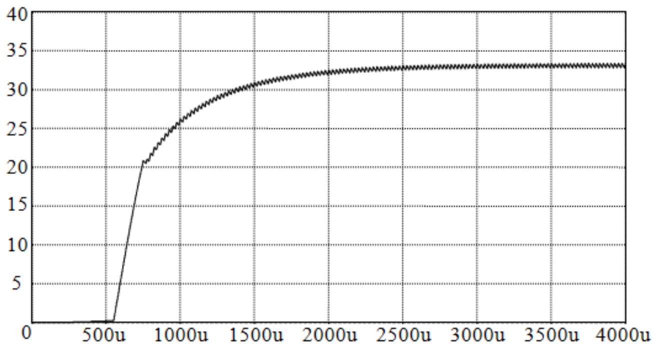

Figure 16. Output voltage for I_{ref}=11*A* (*D*>0.5).

VI. Conclusions

Predictive trailing-edge modulated average current control is deeply investigated in the paper. The control law is derived and theoretical considerations about stability of this type of control are developed. The analysis is carried out in a general manner and therefore the stability conclusions are valid for any converter while the control law is also general and only typical converter values for the slopes need to be inserted to get the digital control law for a given topology. The main contribution and result is that, opposed to the results in [16], it is proven that PDACC is inherently stable for any duty cycle and therefore is a very attractive option. Possible applications are active power factor correction or welding equipment as well. This type of control can be easily implemented using a microcontroller, a DSP or under LabVIEW with proper acquisition boards. Future work will focus on investigating other types of predictive current control, employing leading edge or triangle modulation in conjunction with peak, average or valley current control.

APPENDIX A

MATLAB program for exact simulation of the boost PDACC using TEM

```
clear all; close all; clc;

Vg=10; R=10; L=500e-6; RL=1e-3; C=100e-6; fs=40e3; Ts=1/fs; Iref=11;
Tsim=10e-3; Nmax=Tsim/Ts;
A1=[-RL/L     0;     0    -1/(R*C)]; B1=[1/L; 0]; E1=[0 1; 1 0]; F1=[0; 0];
A2=[-RL/L     -1/L;      1/C    -1/(R*C)]; B2=[1/L; 0]; E2=[0 1; 1 0];
F2=[0; 0];

 I=eye(2);  n=1;
   x(1,n)=0; x(2,n)=1e-6; i(n)=x(1,n); M1(n)=Vg/L; M2(n)=(x(2,n)-Vg)/L;
d(n)=0.1;

 while n<Nmax
     M1(n)=Vg/L; M2(n)=(x(2,n)-Vg)/L; i(n)=x(1,n);
     phi1=expm(A1*d(n)*Ts); psi1=A1\(phi1-I)*B1;
     phi2=expm(A2*(1-d(n))*Ts); psi2=A2\(phi2-I)*B2;
     x(:,n+1)=  phi2*phi1*x(:,n)+(phi2*psi1+psi2)*Vg;
     d(n+1)=-2*(M1(n)+M2(n))/(2*M1(n)+M2(n))*d(n)-
2/((2*M1(n)+M2(n))*Ts)*(i(n)-Iref)+3*M2(n)/(2*M1(n)+M2(n));
         if d(n+1)<0.01
            d(n+1)=0.01;
         elseif d(n+1)>0.99
            d(n+1)=0.99;
         end
     n=n+1;
 end

 plot(d,'-'); xlabel('time [us]'); ylabel('d');
 figure; plot(i,'-'); xlabel('time [us]'); ylabel('iL');
p=10; % last p cycles are represented
k=1; % cycles counter
h=20e-9; % simulation step
counter=0; % end of switching cycle counter
t=0; tsim(1)=0;
m=1; xsim(:,m)=x(:,length(d)-p); phi=expm(A1*h); psi=A1\(phi-I)*B1;
while k<=p
   if ((k-1)*Ts<t)&&(t<=(k-1+d(Nmax-k+1))*Ts)
      phi=expm(A1*h); psi=A1\(phi-I)*B1;
   elseif ((k-1+d(Nmax-k+1))*Ts<t)&&(t<=k*Ts)
      phi=expm(A2*h); psi=A2\(phi-I)*B2;
   end
   xsim(:,m+1)=phi*xsim(:,m)+psi*Vg; tsim(m+1)=tsim(m)+h;
   m=m+1; t=t+h; counter=counter+1;
   if counter==Ts/h
     k=k+1; counter=0;
   else
   end
end
    figure; plot(tsim*1e6,xsim(1,:)); xlabel('time [us]'); ylabel('iL');
```

REFERENCES

[1] C. Deisch, "Simple switching control method changes power converter into a current source," Proc. PESC'78 Conf., pp. 300–306.

[2] S. S. Hsu, A. Brown, L. Rensink, and R. D. Middlebrook, "Modeling and analysis of switching dc-to-dc converters in constant-frequency current programmed mode," in Proc. PESC'79 Conf., pp. 284-301.

[3] F. C. Lee and R. A. Carter, "Investigations of stability and dynamic performances of switching regulators employing current-injected control," Proc. PESC'82 Conf., 1982, pp. 3-16.

[4] L. Dixon, "Average current mode control of switching power supplies," Proc. Unitrode Power Supply Design Sem., 1990.

[5] W. Tang, R. Ridley, and F. C. Lee, "Small-signal analysis of average current-mode control," IEEE Trans. Power Electron., vol. 8, Apr. 1993, pp. 112-119.

[6] A. Chapel, G. Ferrante, D. O'Sullivan, A. Weinberg, "Application of the injected current model for the dynamic analysis of switching regulators with the new concept of LC3 modulator," Proc. IEEE Power Electron. Specialists' Conf., 1978, pp. 135-147.

[7] R. Ridley, "A New Continuous-Time Model for Current-Mode Control", IEEE Trans. Power Electron., vol. 6, no. 2, April, 1991, pp. 271-280.

[8] J. Chen, R. Erickson, and D. Maksimovic, "Averaged switch modeling of boundary conduction mode dc-to-dc converters," Proc. IEEE IECON'01 Conf., 2001, pp. 844–849.

[9] C. Restrepo, J. Calvente, A. Romero, E. Idiarte, R. Giral, "Current-mode control of a coupled-inductor buck-boost dc-dc switching converter", IEEE Trans. Power Electron., vol. 27, no. 5, May 2012, pp. 2536-2549.

[10] R. Redl and N. O. Sokal, "Current-mode control, five different types, used with the three basic classes of power converters: Small-signal ac and large-signal dc characterization, stability requirements, and implementation of practical circuits," Proc. PESC'85 Conf., 1985, pp. 771-785.

[11] W. Tang, F. C. Lee, R. Ridley, I. Cohen, "Charge control: modeling, analysis, and design", IEEE Trans. on Power Electron., Vol. 8, No. 4, Oct. 1993, pp. 396-403.

[12] R. Redl and B. Erisman, "Reducing distortion in peak-current-controlled boost power factor correctors," Proc. IEEE APEC'94 Conf., 1994, pp. 576-583.

[13] D. Maksimovic, "Design of the clamped-current high-power-factor boost rectifier," Proc. APEC'94 Conf., 1994, pp. 584-590.

[14] J. Lai and D. Chen, "Design consideration for power factor correction boost converter operating at the boundary of continuous conduction mode and discontinuous conduction mode," Proc. APEC'93 Conf., 1993, pp. 267-273.

[15] R. W. Erickson and D. Maksimovic, *Fundamentals of Power Electronics*, 2nd ed. Norwell, MA: Kluwer, 2001.

[16] J. Chen, A. Prodic, R. W. Erickson, and D. Maksimovic, "Predictive digital current programmed control," IEEE Trans. Power Electron., vol. 18, no. 1, Jan. 2003, pp. 411-419.

[17] D. Maksimovic, J. Chen, A. Prodic, R. W. Erickson "Predictive digital current controllers for switching power converters", United States patent, Patent No. US 7,148,669 B2, Dec. 12, 2006.

[18] R. Li, T. O'Brien, J. Lee, J. Beecroft, "A unified small signal analysis of dc-dc converters with average current mode control", IEEE Energy Conversion Congress and Exposition, ECCE 2009. pp. 647-654.

[19] F. Yu, F. C. Lee, P. Mattavelli "A small signal model for average current mode control based on describing function approach", Energy Conversion Congress and Exposition, ECCE 2011, pp. 405-412.

[20] D. Sha, Z. Guo, and X. Liao, "Cross-feedback output-current-sharing control for input-series-output-parallel modular DC-DC converters," IEEE Trans. Power Electron., vol. 25, no. 11, Nov. 2010, pp. 2762–2771.

[21] Z. Shen, X. Chang, W. Wang, X. Tan, N. Yan, H. Min, "Predictive digital current control of single-inductor multiple-output converters in CCM with low cross regulation", IEEE Trans. Power Electron., vol. 27, no. 4, April 2012, pp. 1917-1925.

[22] Y. Qiu, X. Chen, and H. Liu, "Digital average current-mode control using current estimation and capacitor charge balance principle for dc–dc converters operating in DCM," IEEE Trans. Power Electron., vol. 25, no. 6, Jun. 2010, pp. 1537–1545.

[23] Y. Yan, F. C. Lee, P. Mattavelli, S. Tian "Small-signal Laplace-domain Model for Digital Predictive Current Mode Controls", IEEE Energy Conversion Congress and Exposition, ECCE 2012, pp. 1386-1393.

[24] S. Ang. A. Oliva, *Power-switching converters*, second edition, CRC press, Taylor & Francis Group, 2005.

[25] CASPOC, user manual, http://www.simulation-research.com

[26] D. Drăghici, "Simulation Aspects in Digital Control of DC-DC Converters", "Interdisciplinaritatea şi managementul cercetării în studiile doctorale",Oradea, România, 7 – 8 iunie 2012, pp. 5.